Met. Mater. Int., Vol. 22, No. 4 (2016), pp. 642~648
doi: 10.1007/s12540-016-6079-5

Ordered Structures in Al-3Cu-(1.78Mg) Alloys Aged at 190 °C for 2 Minutes

Wei Haigen, Xia Fuzhong, Jia Yanlin, and Wang Mingpu*

School of materials science and engineering, Central South University, Changsha 410083, China

(received date: 29 January 2016 / accepted date: 6 March 2016)

Precipitate structures in Al-3Cu (wt%) and Al-3Cu-1.78Mg (wt%) alloys aged at 190 °C for 2 minutes were studied by transmission electron microscopy and high resolution transmission electron microscopy. New models named ordered structures were proposed for the fine precipitates formed in the two aged alloys. Ordered structures in Al-Cu alloys were composed by Al and Cu atoms, and by Al, Cu and Mg atoms together in Al-Cu-Mg alloys. By simulating selected area electron diffraction (SAED) patterns of Al-Cu-(Mg) alloys containing plate-shaped ordered structures and taking into account the influence of the plate shape of ordered structures on their electron diffraction characteristics, [001] zone axis SAED patterns of the two alloys were interpreted. It was concluded that volume expansions of the two aged alloys occurring at the early aging stage are caused by the lattice expansions as ordered structures are formed, and ordered structures are the nuclei for the GP zones in Al-Cu alloys.

Keywords: metals, aging, precipitation, transmission electron microscopy (TEM), ordering

1. INTRODUCTION

Precipitation-hardenable aluminum alloys based on Al-Cu-(Mg) compositions are widely used in structural aerospace applications due to their excellent mechanical properties. Many researches have been conducted to investigate the precipitation hardening mechanisms of the alloys. In the past few years, the rapid hardening effect at the early stages of elevated temperature aging in Al-Cu-Mg alloys has attracted broad attention. For example, atom probe tomography (APT) experiments have demonstrated the formation of "Cu-Mg" clusters in Al-Cu-Mg alloys at the early stages of artificial aging, which were believed to be responsible for the initial rapid age hardening of the alloys [1]. But the employed APT technique cannot reveal whether the "Cu-Mg" clusters have a special crystalline structure. Kovarik *et al*. have affirmed the formation of L10 ordered structures (OSs) at the early aging stage in an Al-3Mg-0.4Cu-0.12Si (wt%) alloy [2], and interpreted their fast fourier transform (FFT) patterns of high resolution transmission electron microscopy (HRTEM) images based on the ordered diffractions from the L10 OSs. On the other hand, in the literature it is widely accepted that GP zones are the initial phases formed during the aging of Al-Cu and low Mg content Al-Cu-Mg alloys [3,4]. But whether or not there are other precipitation structures before GP zones in these alloys has yet to be determined. This may be caused by the small sizes of precipitates before GP zones, which makes precipitate morphology and diffraction intensities hardly identified in HRTEM images and selected area electron diffraction (SAED) patterns, respectively. In fact, diffractions caused by clusters formed at the early aging stages of Al-Cu-Mg alloys had arisen in related SAED patterns [1]. However, they were ignored by the authors due to their weak intensity. In addition, it has been demonstrated that precipitation processes of Al-Li alloys start from the formation of OSs, and OSs are the nuclei for later aging products [5,6]. At present, there are few researches on the role of the clusters formed at the early aging stages in the precipitation processes of Al-Cu-(Mg) alloys. In this paper, we investigate Al-Cu-(Mg) alloys aged at 190 °C for 2 minutes by transmission electron microscopy (TEM) and HRTEM. A new model is proposed to interpret experimental results combing simulation of SAED patterns. At last, we discuss the role of proposed precipitation structures in the aging processes of Al-Cu alloys.

2. EXPERIMENTAL PROCEDURE

Al-3Cu-(1.78Mg) (wt%) ingots were prepared by melting raw materials in a pit furnace under atmosphere. The raw materials used for melting were: 99.7% pure Al, 99.9% pure Cu, and 99.9% pure Mg. After melting, Al-Cu ingots are homogenized at 530 °C, and Al-Cu-Mg ingots at 490 °C for 24 h. After homogenization the two alloys were hot rolled by 80% at 470 °C, then Al-Cu plates were solution treated at 540 °C, and Al-Cu-Mg plates at 500 °C for 1h and quenched into water. After quenching the two alloys were aged at 190 °C in a salt

*Corresponding author: wangmp@csu.edu.cn

bath for 2 minutes. After aging TEM and HRTEM specimens were prepared by cutting a small piece from the aged samples, mechanically grinding to 60–80 μm thickness and then jet polishing in a solution of 30 vol% HNO_3 and 70 vol% CH_3OH at −20 °C. TEM and HRTEM examination were performed using a JEM 2100 at 200 kV. TEM and HRTEM image processing were carried out using Gatan Digital Micro software and simulation of SAED patterns by Crystal Maker software.

3. RESULTS

The [001] zone axis TEM images and SAED patterns of aged Al-Cu and Al-Cu-Mg alloys are shown in Figs. 1(a-b) and Figs. 1(c-d), respectively. As can be seen in Figs. 1(a) and 1(c), after aging lath-shaped precipitates (arrowed in Figs. 1(a) and 1(c)) are formed in the two alloys. In SAED experiments regions as circled in Figs. 1(a) and 1(c) without the lath-shaped precipitates were selected specially. However, in the corresponding SAED patterns shown in Figs. 1(b) and 1(d), besides the fundamental diffractions some weak spots can also be observed, suggesting the presence of very small precipitates

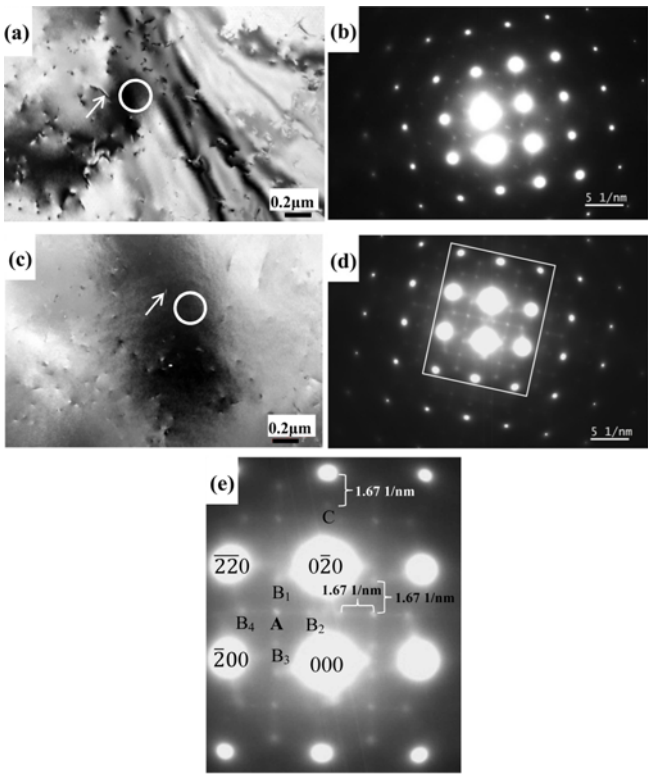

Fig. 1. [001] zone axis TEM images and corresponding SAED patterns of Al-3Cu (a, b) and Al-3Cu-1.78Mg (c, d) alloys aged at 190 °C for 2 minutes. The circled regions in (a) and (b) without the lath-shaped particles arrowed in the two figures are the selected areas for SAED. The region marked by a rectangle in (d) is amplifiedly shown in (e) should be revised also, because the yellow background of the text in Fig. 1(e) of the last version was set to indicate that it was changed according to the reviewers' comments.

in the circles regions in Figs. 1(a) and 1(c). In addition, in our experiments it was found that, no matter which regions without the lath-shaped precipitates were selected for [001] zone axis SAED observations, the same results as Figs. 1(b) and 1(d) were always obtained for the two aged alloys, indicating that the tiny precipitates which are indistinguishable in TEM bright field images exist everywhere in the two aged alloys. Figures 1(b) and 1(d) also show that equal SAED patterns are obtained for the two alloys, except that the diffraction intensities from precipitates in the Al-Cu-Mg alloy are higher than that from the Al-Cu alloy. To facilitate illustration and discussion in the following, the area marked by a rectangle in Fig. 1(d) is amplifiedly shown in Fig. 1(e) and diffractions from precipitates are classified into three groups in this figure, namely A, B and C-type diffractions. A-type diffractions locate at {110} positions, around which four B-type diffractions locate. C-type diffractions locate on <0 2n 0> directions and have an equal distance (1.67 1/nm) from one (0 2n 0) spot as that of B-type diffractions from a A-type diffraction, as indicated in Fig. 1(e). The C-type spots can only be observed at positions far from the image center where background noise is not too high to conceal them.

The A-type diffractions were thought to be caused by L10 OSs composed by Cu and Mg atoms, without Al [2]. But if L10 OSs exist in our alloys, {010} supperlattice spots should also be present in the [001] zone axis SAED patterns, as shown in Fig. 2 which shows the simulated [001] zone axis SAED pattern of the L10 OS. In addition it is impossible for the L10 OSs composed by Cu and Mg atoms to exist in the Al-Cu alloy. So the A-type diffractions in Figs. 1(b) and 1(d) cannot be interpreted by L10 OSs. In the literature the A and B-type diffractions observed in the SAED patterns of aged Al-Cu-Mg alloys are thought by some authors to be caused by S" phases composed by Al, Cu and Mg atoms [2,7], and they are also attributed sometimes to Al_2O_3 formed during TEM specimen preparation by some authors [8,9]. But these interpretations cannot explain the C-type diffractions in Figs. 1(b) and 1(d). In addition it was found in our experiments that the three types of diffractions are characteristic of the early aging precipitates in the two alloys. If the two alloys are over aged to 1000 minutes,

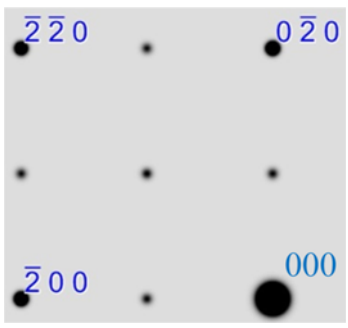

Fig. 2. The simulated [001] zone axis SAED pattern of L10 ordered structures.

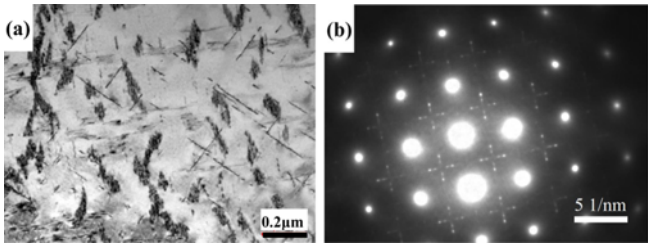

Fig. 3. The [001] zone axis TEM image and corresponding SAED pattern of Al-3Cu-1.78Mg alloy aged at 190 °C for 1000 minutes.

completely different SAED patterns from that shown Figs. 1(b) and 1(d) will be obtained. Figure 3 shows the [001] zone axis TEM image and SAED pattern of the Al-Cu-Mg alloy aged 190 °C for 1000 minutes. It can be seen in Fig. 3(a) that many precipitates about 1μm are formed at this aging stage, which can be judged as S' phases from the SAED pattern shown Fig. 3(b) [10]. The above illustration indicates that the three types of diffractions in Figs. 1(b) and 1(d) are caused by the aging products formed at the early aging stages of the two alloys. Here we further conclude that the same or similar precipitates are formed in the two alloys at this stage because almost the same SAED patterns are obtained.

In order to observe the tiny precipitates giving rise to the three types of diffractions in SAED patterns in Figs. 1(b) and 1(d), the two alloys are observed by HRTEM and images of Al-Cu and Al-Cu-Mg alloys are shown in Figs. 4(a) and 4(b), respectively. In the two images areas marked by green rectangles are where the lath-shaped particles as arrowed in Figs. 1(a) and 1(c) locate, and areas marked by red rectangles are the matrix areas without the lath-shaped particles as circled in Figs. 1(a) and 1(c). FFT results of these marked regions are shown in Figs. 4(c-f). Even though no precipitates with clear morphology can be found in the matrix areas marked by red rectangles in Figs. 4(a) and 4(b), {110} A-type diffractions are present in the corresponding FFT patterns shown in Figs. 4(d) and 4(f), indicating the presence of tiny clusters in the alloy matrices. It has been demonstrated that clusters are formed in Al-Cu-(Mg) alloys at the early aging stages [1], even though the structures of these clusters were not identified there. Again it was found in our experiments that no matter which matrix regions in the HRTEM patterns of the two alloys were selected for FFT, A-type diffractions always existed in obtained FFT images. Comparison between Figs. 4(c) and 4(d) indicates that the same precipitation structures are formed in regions with and without the lath-shaped particles in the Al-Cu alloy, because the same FFT patterns are obtained for the two regions. Figure 4(e) indicates that the lath-like particles in the Al-Cu-Mg alloy are S' phases [10]. In experiments it was also found that, if a large area of alloy matrices were selected from the HRTEM images of the two alloys to perform FFT so as to increase the signal to noise ratios of FFT patterns, not only A-type but also B-type diffractions could be observed in FFT patterns. Figure 4(g) shows a

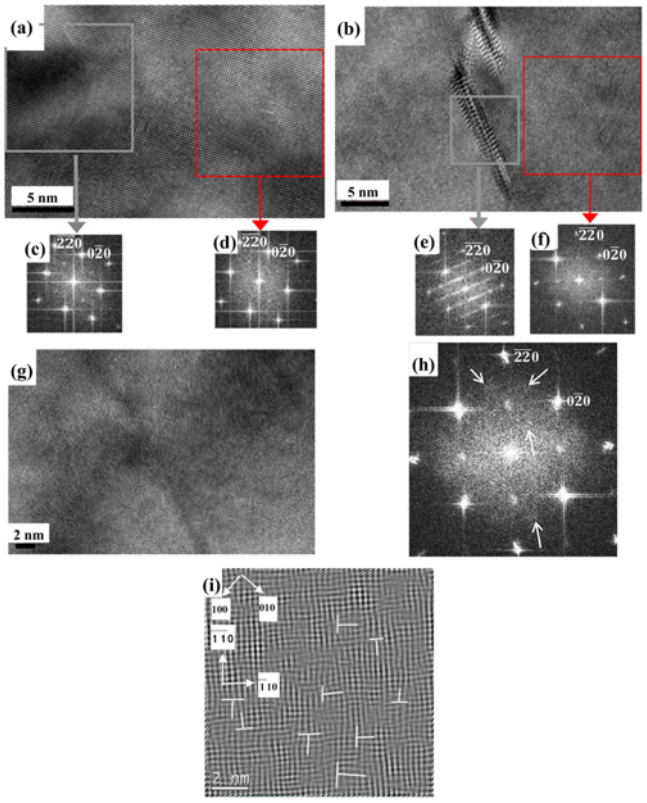

Fig. 4. [001] zone axis HRTEM images of Al-3Cu (a) and Al-3Cu-1.78Mg (b) alloys aged at 190 °C for 2 minutes. In the two images areas marked by green rectangles are where the lath-shaped particles as arrowed in Figs. 1(a) and 1(c) locate, and areas marked by red rectangles are the matrix areas without the lath-shaped particles. FFT patterns of these marked regions are shown in (c-f). (g) A HRTEM image of Al-Cu-Mg alloy matrix without lath-shaped precipitates. (h) The FFT pattern obtained by selecting the whole image (g) to perform FFT, in which B-type diffractions are arrowed. (i) The image obtained by selecting the four {110} A-type diffractions in (f) to perform inverse fast fourier transformation, in which some edge dislocations with one extra {110} half plane are indicated.

HRTEM image of the Al-Cu-Mg alloy matrix without lath-shaped precipitates. By selecting this whole HRTEM image to perform FFT a pattern with A and B-type diffractions is obtained, as shown in Fig. 4(h), in which the B-type diffractions are arrowed. By selecting the four {110} A-type diffractions in Fig. 4(f) to perform inverse fast fourier transformation (IFFT), an image containing some edge dislocations with one extra {110} half plane is obtained, as indicated in Fig. 4(i). In this image the projection lines of two sets of crystal planes are indicated by arrows. Because a perfect edge dislocation in a face center cubic (FCC) crystal contains two extra {110} half planes [11], these dislocations in Fig. 4(i) can be judged as imperfect dislocations.

4. DISSCUSSION

In order to interpret our TEM and HRTEM results, a new

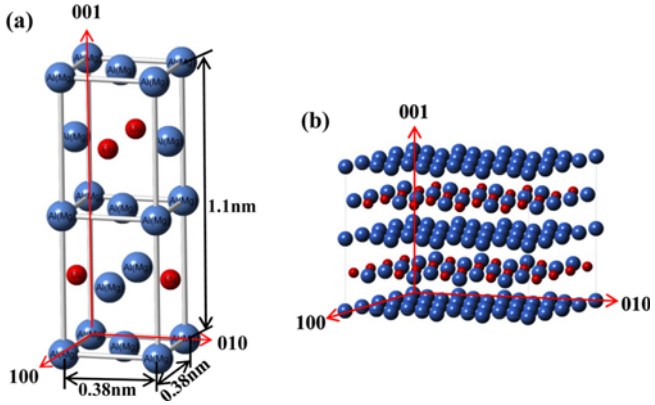

Fig. 5. (a) A model for the precipitates formed in Al-Cu-(Mg) alloys at the early aging stage, which is called the ordered structure (OS). For the OS in the Al-Cu alloy, blue atoms are Al atoms and red atoms Cu atoms. For the OS in the Al-Cu-Mg alloy, some Al atoms are replaced by Mg atoms. (b) The plane-shaped OS.

Table 1. Crystal parameters of and atomic occupancy in the OS shown in Fig. 5(a)

Spacegroup: I-4 m2		X	Y	Z
a = 0.38 nm	Al(Mg)	0.5	0.5	0
b = 0.38 nm	Al(Mg)	0	0	0
c = 1.1 nm	Al(Mg)	0.5	0	0.25
α = β = γ = 90°	Cu	0	0.5	0.25

model for the tiny precipitates formed at the early aging stages in Al-Cu-(Mg) alloys is proposed, as shown in Fig. 5(a). Here we term this precipitation structure OS because we think it is formed very quickly at the early aging stage by local atomic ordering which does not need long range atomic diffusion. The crystal parameters of and atomic occupancy in the OS are shown in Table 1. The OS has a cubic-cubic orientation relationship with Al matrix, that is $[100]_{Al}//[100]_{OS}$, $[010]_{Al}//[010]_{OS}$ and $[001]_{Al}//[001]_{OS}$. For the OS in the Al-Cu alloy, blue atoms in Fig. 5(a) are Al atoms and red atoms are Cu atoms. By replacing some Al atoms in the OS of the Al-Cu alloy by Mg atoms, the OS in the Al-Cu-Mg alloy can be obtained. The higher the Mg content of an Al-Cu-Mg alloy, the more the Al atoms are replaced by Mg. Because Mg atoms have an almost equal electron scattering factor to Al atoms [12], SAED patterns with equal precipitate diffractions are obtained for the two alloy matrices containing OSs, as shown in Figs. 1(b) and (d). Furthermore since Mg can promote the precipitation process of Cu [1], more OSs will be formed in the Al-Cu-Mg alloy than in the Al-Cu alloy, causing higher diffraction intensities of OSs in the Al-Cu-Mg alloy than in the Al-Cu alloy, as shown in Figs. 1(b) and 1(d). In the literature it has been revealed that during the aging of Al-Cu-(Mg) alloys, the first process occurring is the segregation of Cu atoms on $\{001\}_{Al}$ planes to formed plane-shaped precipitates [13,14]. In the model shown in Fig. 5(a) Cu atoms locate on two separated $(001)_{Al}$ planes. However because it is the aging product formed at the early aging stage, not all the Al atoms on the Cu segregation planes have diffused out the OS. Hereinafter the Cu atom segregation plane of the OS will be referred to as OS plane. By spreading the OS in Fig. 5(a) in directions parallel to the OS plane, a plane-shaped OS with morphology being more consistent with the literature is obtained, as shown in Fig. 5(b).

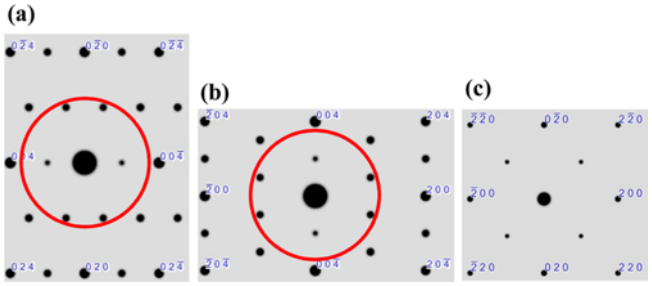

Fig. 6. Simulated SAED patterns of OSs with their (a) [100], (b) [010] and (c) [001] crystal directions parallel to the incident electron beam, respectively. Spot sizes in these patterns represent the kinetic diffraction intensities of corresponding crystal planes. The spots in circled regions of (a) and (b) are those that are proposed to be visible in experimental SAED patterns as the influence of the plane-shape of ordered structures on electron diffraction is considered, as shown in Fig. 7.

Along the $[001]_{Al}$ zone axis, there are three types of OS variants participating electron diffraction. The simulated SAED patterns of the three variants with their [100], [010] and [001] crystal directions parallel to the incident electron beam are shown in Figs. 6(a-c), respectively. In these patterns spot sizes represent the kinetic diffraction intensities of corresponding crystal planes. The patterns shown in Figs. 6(a) and 6(b) come from the OS variants with their OS planes parallel to the incident electron beam, as shown in Fig. 7(a). In this case, OS diffractions will elongate perpendicular to and contract parallel to the OS plane, as shown in Fig. 7(a). This diffraction spot distortion may make those OS diffractions far from the image center invisible in experimental SAED patterns as the rel-rods of these diffractions cannot intersect or intersect only a short length with the Ewald sphere, as shown in Fig. 7(a). Here we assume that, in practice, for the OS variants which should give rise to SAED patterns as Fig. 6(a) and 6(b), only these circled diffractions in the two figures are visible in experimental SAED patterns. On the other hand, for the OS variants whose OS planes are perpendicular to the incident electron beam, theoretically speaking, a SAED pattern as shown Fig. 6(c) should be caused. In view of the diffraction spot elongation perpendicular to the OS plane, diffraction intensities from the OS variants may be strengthened in practice, as shown in Fig. 7(b). At last, if OS variants locate in such an orientation that their OS planes slightly deviate from the incident electron beam, the OS diffraction intensities on one side of SAED patterns will be increased because the rotation of rel-rods with the OS variants increases their intersection lengths with the Ewald sphere, as shown in Fig. 7(c).

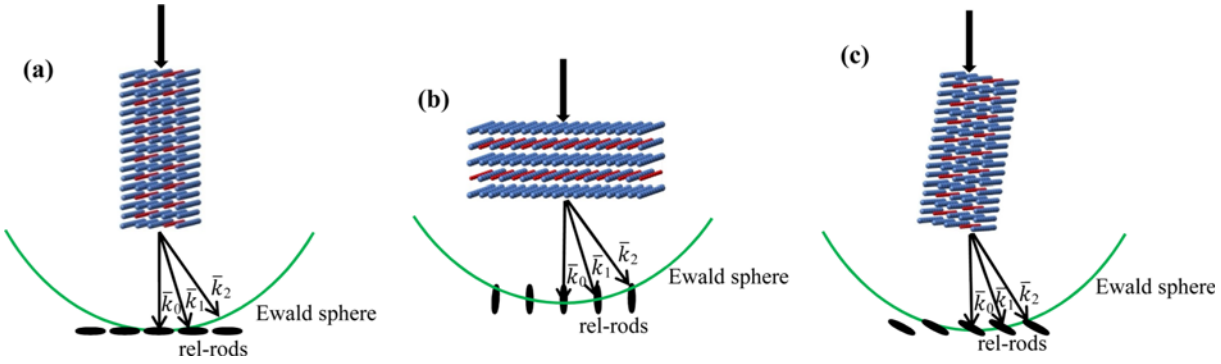

Fig. 7. The influence of diffraction spot elongation perpendicular to the OS planes caused by the plane shape of ordered structures on the diffraction intensities. (a) The case in which the [100] or [010] crystal direction of the OS is parallel to the incident beam, making the OS diffractions far from the image center invisible. (b) The [001] direction of the OS is parallel to the incident beam, increasing the intersect lengths of rel-rods with the Ewald sphere and diffraction intensities of OS diffractions. (c) The [100] or [010] direction of the ordered structure is slightly deviated from the incident beam, increasing the OS diffraction intensities on one side of the SAED patterns with respect to that in (a).

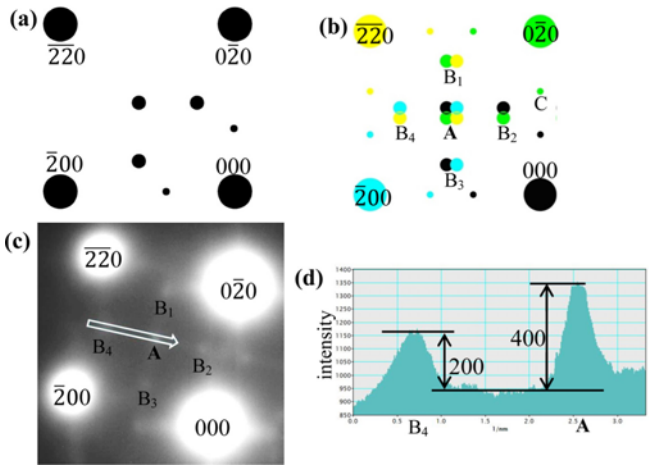

Fig. 8. (a) The SAED pattern obtained by overlapping the circled regions in Figs. 6(a) and 6(b) with Fig. 6(c). (b) The simulated SAED pattern of Al-Cu-(Mg) alloys containing OSs with electron double diffraction considered, which is obtained by plotting the same patterns as (a) with $(0\bar{2}0)_{Al}$, $(\bar{2}\,\bar{2}0)_{Al}$ and $(\bar{2}00)_{Al}$ diffraction spots in (a) as incident beams and overlapping the obtained three patterns with (a). (c) Part of Fig. 1(e) in which an arrow shows the intensity computing line with the arrow width representing the computing width. (d) The intensity computing result of (c) along the arrow from the B_4 to A spot.

By overlapping the circled regions in Figs. 6(a) and 6(b) with Fig. 6(c), the simulated [001] zone axis SAED pattern of Al-Cu-(Mg) alloys containing three types of plane-shaped OS variants is obtained, as shown in Fig. 8(a). In this pattern electron double diffraction is not taken into account. By plotting the same patterns as Fig. 8(a) with $(0\bar{2}0)_{Al}$, $(\bar{2}\,\bar{2}0)_{Al}$ and $(\bar{2}00)_{Al}$ diffraction spots in Fig. 8(a) as the incident beams and overlapping the obtained three patterns with Fig. 8(a), the simulated SAED pattern with electron double diffraction considered is obtained, as shown in Fig. 8(b). This simulated pattern is consistent with Fig. 1(e), except that the C-type diffractions are visible in Fig. 1(e) only at the positions far from the image center. This disagreement is due to two reasons. First, it is indicated in Fig. 8(a) that the kinetic diffraction intensities of C-type diffractions are weaker than that of A and B-type diffractions. Second, it is illustrated in Fig. 8(b) that each A and B-type spots in experimental patterns are formed by overlapping of 4 and 2 diffraction beams, respectively, whereas each C-type spot is formed by only one diffraction beam. So in practice the C-type diffractions are hardly visible at the image center with high background noise. On the other hand, as illustrated in Figs. 6(a) and 6(b), C-type diffractions come from the OS variants whose OS planes are parallel to the incident beam. In these cases, if a slightly deviated incident beam is applied, the C-type diffractions may be visible in experimental SAED patterns owing to the increased intersection lengths of their rel-rods, as shown in Fig. 7(c). In Fig. 1(e), taking the $(0\bar{4}0)_{Al}$ diffraction beam as incident beam to give rise to the C-type diffractions just meets this inclined illumination requirement, and along with the low background noise near the $(0\bar{4}0)_{Al}$ diffraction, the C-type diffraction spot can be observed near the $(0\bar{4}0)_{Al}$ diffraction. By computing the electron intensity distribution in Fig. 1(e) along the line from the B_4 to A spot, as shown in Fig. 8(c), it is found that, after deducting the background noise, the electron intensity of the A spot is twice that of the B_4 spot, as shown in Fig. 8(d), being in accordance with the simulated results shown in Fig. 8(b). For this reason, the B-type diffractions weaker than the A-type diffractions cannot be observed in the FFT patterns of HRTEM images of Al-Cu-(Mg) alloy matrices shown in Figs. 4(d) and 4(f). Only by selecting a large area of HRTEM image to perform FFT so as to increase the signal to noise ratio in FFT patterns, can the B-type diffractions be observed, as shown in Fig. 4(h).

It was found by Glossop and Pashley that some imperfect dislocations may exist at the interfaces between two OSs to relieve interfacial strain [15]. The dislocations in Fig. 4(i) having only one extra {110} half plane may be this kind of interfacial dislocations. From Table 1 we find that the volume of

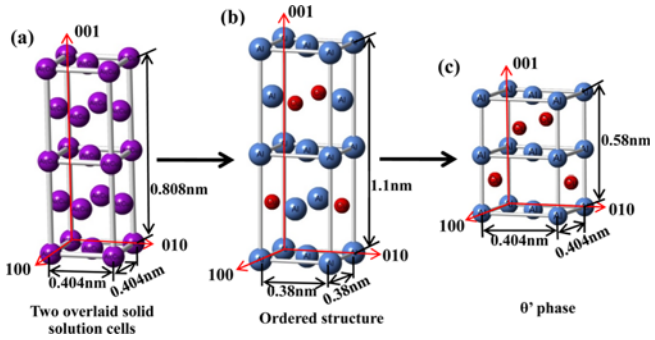

Fig. 9. The proposed aging sequences of Al-Cu alloys. (a) Two overlaid solid solution unit cells obtained by quenching in which Al and Cu atoms occupy the lattice sites randomly. (b) The OS formed at the early aging stage in which Cu atoms segregate on two separated $(001)_{Al}$ planes with some Al atoms on the Cu atom segregation planes retained. (c) The unit cell of θ' phase formed as Al atoms on the Cu segregation planes diffuse out the OS with aging.

an OS unit cell is 0.1795376 nm^3, which is larger than that of two Al unit cells, which is 0.1318786 nm^3, suggesting that lattice expansion occurs with the formation of OSs during aging. In the literature, volume expansions occurring at the early aging stages of Al-Cu-(Mg) alloys have been found by some authors [16,17], which can be explained based on the model we proposed here. However, if only the lattice contractions occurring with the segregation of Cu atoms on $\{001\}_{Al}$ planes during the aging of Al-Cu-(Mg) alloys are considered [18], it is volume contraction other than expansion that should be caused, which is not the true case.

GP zones in Al-Cu alloys give rise to the intensity streaks passing through the fundamental spots in the <001> directions [4]. In Fig. 1(b) we cannot find this evidence for GP zones. On the other hand, it is impossible the formation stage of GP zones in the Al-Cu alloy has been passed after aging at 190 ℃ for 2 minutes. So the OSs which give rise to the three types of precipitate diffractions in Fig. 1(b) can only be regarded as the nuclei for GP zones. Based on this we conclude the precipitation sequences in the Al-Cu alloy as solid solution → OSs → GP zones → θ', as shown in Fig. 9. Figure 9(a) shows two overlaid solid solution unit cells in which Al and Cu atoms occupy the lattice sites randomly. During the early aging stage, Cu atoms segregate on separated $(001)_{Al}$ planes by short range atomic diffusion with some Al atoms on the Cu atom segregation planes retained, because longer aging time is needed for all Al atoms to diffuse out the planes. This segregation process leads to the formation of OS shown in Fig. 9(b). With these Al atoms on the Cu segregation planes diffusing out the OS during aging, a more stable structure is formed, as shown in Fig. 9(c), which is consistent with the structure of θ' phase [19,20]. It has been illustrated that in Al-Cu alloys θ' phases are formed from GP zones [21]. From Fig. 9 we can conclude that GP zones are the intermediate aging products from OSs to θ' phases. The multi-layer GP zones observed in the literature at the early aging stages of Al-Cu alloys may be the OSs that have not transformed to GP zones [13,22].

5. CONCLUSIONS

In order to interpret the TEM and HRTEM results, a new model for the precipitates formed at the early aging stages of Al-Cu-(Mg) alloys was proposed, which was called the OS. The formation of the OS is accomplished by the segregation of Cu atoms on $\{001\}_{Al}$ planes which does not need long range atomic diffusion. The OS has a plane shape which can cause diffraction spot elongation perpendicular to the OS plane. By taking into account this diffraction spot elongation and double diffraction, [001] zone axis SAED patterns of Al-Cu-(Mg) alloys containing OSs were simulated, which were consistent with the experimental ones. Diffraction intensity distributions in experimental SAED patterns and their differences from the FFT patterns of alloy matrices could also be interpreted based on the simulated results. It was concluded that the lattice extensions accompanying the formation of OSs are the causes of volume extensions of Al-Cu-(Mg) alloys occurring at the early aging stages, and OSs are the nuclei for GP zones in Al-Cu alloys.

ACKONWLEDGEMENTS

This work was supported by Grants from the Project of Innovation-driven Plan in Central South University.

REFERENCES

1. R. K. W. Marceau, G. Sha, R. Ferragut, A. Dupasquier, and S. P. Ringer, *Acta. Mater.* **58**, 4923 (2010).
2. L. Kovarik, P. I. Gouma, C. Kisielowski, S. A. Court, and M. J. Mills, *Acta. Mater.* **52**, 2509 (2004).
3. S. Abis, M. Massazza, P. Mengucci, and G. Riontino, *Scr. Mater.* **45**, 685 (2001).
4. T. J. Konno, M. Kawasaki, and K. Hiraga, *Philos. Mag. B* **81**, 1713 (2001).
5. Y. Ohmori, K. Nakai, and S. Ito, *Metall. Mater. Trans. A* **30**, 741 (1999).
6. R. Yoshimura, T. J. Konno, E. Abe, and K. Hiraga, *Acta. Mater.* **51**, 2891 (2003).
7. S. C. Wang and M. J. Starink, *Mat. Sci. Eng. A* **386**, 156 (2004).
8. V. A. Phillips, *Acta. Mater.* **23**, 751 (1975).
9. J. K. Park and A. J. Ardell, *Metall. Mater. Trans. A* **14**, 1957 (1983).
10. C. B. Zhang, W. Sun and H. Q. Ye, *Phil. Mag. Lett.* **59**, 265 (1989).
11. J. S. Pan, *The Fundamentals of Materials Science*, p.277, TsingHua University Press, BeiJing (2007).
12. D. B. Williams and C. B. Carter, *Transmission Electron Microscopy: A Textbook for Materials Science*, p. 39, Plenum Press, New York (1996).

13. E. Matsubara and J. B. Cohen, *Acta. Mater.* **33**, 1957 (1985).
14. L. Kovarik and M. J. Mills, *Scr. Mater.* **64**, 999 (2011).
15. A. B. Glossop and D. W. Pashley, *P. Roy. Soc. Lond. A. Mat.* **250**, 132 (1959).
16. W. Fink, D. Smith and L. Willey, *Age Hardening of Metals*, pp.31-55, Tower Press, Cleveland (1940).
17. H. Hardy, *J. Inst. Met.* **83**, 17 (1954).
18. V. Gerold, *Scr. Mater.* **22**, 927 (1988).
19. G. Lorimer, K. Russell, and H. Aaronson, *Precipitation Processes in Solids*, pp. 87-119, Metallurgical Society of AIME, Warrendale, Pa (1978).
20. S. C. Wang and M. J. Starink, *Int. Mater. Rev.* **50**, 193 (2005).
21. H. Fujita and C. Lu, *Mater. Trans.* **33**, 892 (1992).
22. K. Höno, T. Satoh and K. Hirano, *Philos. Mag. A* **53**, 495 (1986).